16th AIAA Computational Fluid Dynamics Conference
23-26 June 2003, Orlando, Florida

AIAA 2003-3685

Application of least-squares spectral element methods to incompressible flow problems

M. M. J. Proot* & M. I. Gerritsma† & M. Nool‡

Least-squares spectral element methods are based on two important and successful numerical methods: spectral/*hp* element methods and least-squares finite element methods. In this respect, least-squares spectral element methods are very powerfull since they combine the generality of finite element methods with the accuracy of the spectral methods and also the theoretical and computational advantages in the algorithmic design and implementation of the least-squares methods. The present paper continues the development of the least-squares spectral element methods by concentrating on the application of this method to incompressible flow problems. Therefore, the derivation of the least-squares spectral element fomulation of the velocity-vorticity-pressure form of the unsteady Navier-Stokes equations plays a central role in the present paper. Moreover, the numerical simulation of the lid driven cavity problem confirms that the least-squares spectral element method produces spectrally accurate results.

1. Introduction

SPECTRAL element methods combine the generality of finite element methods with the higher order accuracy of the solution due to the high-order basis-functions.[1] Consequently, since these methods are often associated with high-order finite element methods, they are called *hp*-finite element methods.[2] In comparison with finite element methods, spectral element methods need less degrees of freedom to obtain a prescribed level of accuracy, but the amount of work per degree of freedom which needs to be done is higher. Since spectral element methods are a subclass of finite element methods, weak formulations for the spectral element method may be obtained by Galerkin's method.

Recently, the spectral element discretization of the incompressible Navier-Stokes equations has received much attention.[2,3] In the weak formulation, one needs to define approximating function spaces for the velocity and pressure. However, the velocity and pressure cannot be approximated independently due to the well known Ladyzhenskaya-Babuška-Brezzi compatibility condition.[4] This condition can be satisfied by reducing the polynomial degree for the pressure. A well known compatible velocity-pressure combination is the so-called $P_N \times P_{N-2}$ formulation of Bernardi and Mayday.[5,6] Moreover, the resulting discrete system is derived from a saddle point problem and is difficult to solve numerically. To overcome this, the discrete governing equations are often decoupled by using projection methods or generalized block LU-decompositions.

For many engineering problems, the least-squares formulation provides an attractive alternative to the standard Galerkin formulation. Irrespective of the type of the underlying partial differential equation, the least-squares formulation always leads to symmetric algebraic systems, which means that only half of the coefficients need to be stored. If, in addition, the system satisfies an a priori coercivity inequality, the least-squares formulation generates positive definite algebraic matrices, which allow for the use of well-established solvers, such as preconditioned Conjugate Gradient methods. Furthermore, for mixed problems, such as the incompressible Stokes and Navier-Stokes equations, compatibility conditions between the various approximating function spaces can be circumvented.[4] The method remains symmetric, positive definite for the non-linear Navier-Stokes equations when a continuation technique with respect to the Reynolds number is properly implemented.[7]

Is has been shown[4,8,9] that it is possible to combine the generality of finite element methods with the accuracy of the spectral methods and also the theoretical and computational advantages in the algorithmic design and implementation of least-squares methods. Indeed, the least-squares spectral element method has been developed to achieve this goal. Recent results[4,8,9] reveal that the least-squares spectral element method provides the same order of accuracy as the Galerkin spectral element method. To this end, a nodal representation based on the Legendre[4,8,9] or Chebyshev[10] polynomials can be used to expand the approximate solution. However, the governing equations must, be transformed into an equivalent first order system to mitigate continuity requirements between neighbouring finite elements and to keep the condition number of the resulting discrete system under control.[11]

*Delft University of Technology, Department of Aerospace Engineering, P.O. Box 5058, 2600 GB Delft, The Netherlands
†Delft University of Technology, Department of Aerospace Engineering, P.O. Box 5058, 2600 GB Delft, The Netherlands
‡CWI, P.O. Box 94079, 1090 GB Amsterdam, The Netherlands

The present paper deals with the application of the least-squares spectral element method to incompressible flow problems. In Section 2, the least-squares spectral element method is discussed for an abstract boundary value problem. In particular, the fully coercive least-squares method with strongly imposed boundary conditions is treated. Also some practical aspects are discussed in this section. In Section 3, the theory is applied to the unsteady Navier-Stokes equations to obtain the least-squares formulation. The velocity-vorticity-pressure formulation is used in the present paper. The numerical results are discussed in the subsequent section (Section 4). To this end, the lid driven cavity problem is simulated at a Reynolds number of 1000 and the results are compared with the commonly used benchmark results of Botella and Peyret.[12] The last section is devoted to the conclusions.

2. The least-squares formulation

The principle of least-squares methods is first discussed for an abstract boundary value problem with strongly imposed boundary conditions. An important aspect in the theoretical analysis of least-squares formulations is to establish the equivalence between the residual of the differential equation in a certain norm and the error with respect to the exact solution in a corresponding norm. This equivalence will be elaborated upon in the next section. From the equivalence between the residual norm and the corresponding error norm, a priori error estimates can be derived.

Consider the following abstract boundary value problem

$$\mathcal{L}(U) = F \text{ in } \Omega \tag{1}$$

$$\mathcal{R}(U) = G \text{ on } \Gamma \tag{2}$$

in which $\mathcal{L}$ is a linear first order partial differential operator acting on a scalar or a vector U of unknowns; F is a given vector-valued function; $\mathcal{R}$ is a trace operator acting on the functions U and G represents a given vector-valued function on the boundary. Without any loss of generality, one can take $G = 0$. If the governing equations involve second or higher order derivatives, the scalar equation or system will *first* be transformed into a first order system.

Fully coercive least-squares methods with strongly imposed boundary conditions

It is assumed that the system given by (1)-(2) is well-posed and that the operator $\mathcal{L}$ is a continuous mapping from the underlying Hilbert space X onto a Hilbert space Y, i.e. there exists a positive constant M, independent of U, such that for all $U \in X$ the mapping $\mathcal{L}$ satisfies

$$\|\mathcal{L}(U)\|_Y \leq M \|U\|_X \quad \forall U \in X \ , \tag{3}$$

and, additionally, we require that the mapping possesses a continuous inverse, which can be expressed by

$$\alpha \|U\|_X \leq \|\mathcal{L}(U)\|_Y \quad \forall U \in X \ , \tag{4}$$

where α is a positive constant independent of U. The space X consists of functions which already satisfy the boundary condition (2) with $G = 0$. Note that by virtue of the estimate (3) and (4), the norms $\|U\|_X$ and $\|\mathcal{L}(U)\|_Y$ are equivalent. The coercivity relation (4) is of paramount importance for the minimizing principle of least-squares methods. To appreciate this, assume that the function $U - U_e$ is measured by means of the estimate (4) where $U_e \in X$ represents the "exact" solution of the boundary value problem (1)-(2). Since $\mathcal{L}$ is a linear operator, and since U_e represents the exact solution, the estimate (4) can be recast into

$$\alpha \|U - U_e\|_X \leq \|\mathcal{L}(U) - F\|_Y , \qquad \forall U \in X. \tag{5}$$

This inequality leads to the very important observation that if the norm of the residual of (1) approaches zero ($\|\mathcal{L}(U) - F\|_Y \to 0$), the approximate solution converges to the exact solution ($\|U - U_e\|_X \to 0$). This is the reason why it makes sense to minimize the residual $\mathcal{L}(U) - F$ in the Y-norm in order to obtain a good approximate/numerical solution. The unique minimizer of the quadratic least-squares functional

$$\mathcal{I}(U) = \frac{1}{2} \|\mathcal{L}(U) - F\|_Y^2 \qquad \forall U \in X, \tag{6}$$

solves the boundary value problem (1)-(2). The minimization of the quadratic least-squares functional (6) written as

$$\text{Seek } U \in X \text{ such that } \mathcal{I}(U) \leq \mathcal{I}(V), \quad \forall V \in X, \tag{7}$$

can be obtained by means of the Euler-Lagrange equation

$$\delta\mathcal{I}(U) = \lim_{\varepsilon \to 0} \frac{d}{d\epsilon} \mathcal{I}(U + \epsilon V) = 0, \qquad \forall V \in X, \tag{8}$$

applied to the quadratic least-squares functional (6) which subsequently results into the following weak formulation

$$\begin{gathered} \text{Seek } U \in X \text{ such that} \\ B(U, V) = F(V), \quad \forall V \in X, \end{gathered} \tag{9}$$

where $B(U,V) = (\mathcal{L}(U), \mathcal{L}(V))$ and $F(V) = (F, \mathcal{L}(V))$. Since $B(\cdot,\cdot)$ is symmetric, continuous and coercive in X by relation (4) and since $F(\cdot)$ is continuous, the weak formulation (9) has a unique solution by virtue of the Lax-Milgram lemma.[4]

The last step in the derivation of the abstract boundary value problem consists of choosing a suitable finite-dimensional subspace $X^h \subset X$ which yields the discrete variational problem

$$\begin{gathered} \text{Seek } U^h \in X^h \text{ such that} \\ B\left(U^h, V^h\right) = F\ \left(V^h\right), \quad \forall V^h \in X^h \end{gathered} \tag{10}$$

where the superscript h represents a grid parameter (h is the mesh spacing for finite element methods or the reciprocal of the polynomial degree of spectral methods). In the present work only conforming spectral element discretizations are considered.[2,4,8,9]

Practical aspects

From a practical point of view, only least-squares formulations which allow for the use of C^0-spectral elements are usable. Since C^0-finite or spectral element methods are based on piecewise continuously differentiable polynomials, standard finite and spectral elements can be used which results in a very practical method from an implementational point of view. This can be accomplished by *first* transforming the system into a first order system and subsequently requiring that only (scaled) L^2-norms are used in the quadratic least-squares functional. The transformation into a first order system has two important consequences. First of all, the continuity requirements between neighboring spectral elements will be mitigated such that C^0-finite or spectral elements can be used (in case the residuals are measured by L^2-norms). Secondly, the transformation will keep the condition number of the resulting discrete system under control.[13]

3. The least-squares formulation of the unsteady Navier-Stokes equations

For unsteady incompressible flows with constant dynamic viscosity, the governing equations are the Navier-Stokes equations. These equations are characterized by the fact that the momentum equations (e.g. equations (11)) are coupled to an incompressibility constraint which states that the velocity vector field is divergence free, (e.g. equation (12)). In terms of the primitive variables $(\mathbf{u}, p)$ the governing equations read

$$\frac{\partial \mathbf{u}}{\partial t} + (\mathbf{u}\cdot\nabla)\,\mathbf{u} = -\nabla p + \nu\Delta\mathbf{u} + \mathbf{f} \quad \text{in } \Omega\,, \tag{11}$$

$$\nabla\cdot\mathbf{u} = 0 \quad \text{in } \Omega\,, \tag{12}$$

where $\mathbf{u}$ represents the velocity vector, p the kinematic pressure, $\mathbf{f}$ the forcing term per unit mass (if applicable) and ν the kinematic viscosity. In the present paper, the Navier-Stokes equations (11)-(12) are solved with velocity boundary conditions only.

The importance of the a priori estimate for the *first order* least-squares formulation has been discussed in the previous section. As discussed above, one must transform the Navier-Stokes equations equation (11)-(12) into an equivalent first order system. Five different first order formulations of the Stokes equations have been assessed in the context of the least-squares spectral element method in the dissertation of Proot.[4] This discussion revealed that the velocity-vorticity-pressure formulation is a good compromise between accuracy and practicality. Indeed, this formulation recovers full accuracy for all the variables with some boundary conditions and the formulation can be supplemented with a number of non-standard boundary conditions that are easy to impose in a strong sense. Moreover, numerical experience with least-squares *finite* element methods based on this formulation[13–24] revealed that the method remained sufficiently accurate even when it was not fully optimal. With these considerations in mind, it has been decided to develop a least-squares spectral element method based on the velocity-vorticity-pressure formulation.

A thorough discussion on the function spaces to be used in combination with various types of boundary conditions can be found in the work of Proot & Gerritsma.[9]

The first order formulation of the Navier-Stokes equations

In order to obtain the velocity-vorticity-pressure formulation of the unsteady Navier-Stokes equations, the vorticity ω has been introduced as an auxiliary variable. By using the identity $\nabla\times\nabla\times\mathbf{u} = -\Delta\mathbf{u}+\nabla(\nabla\cdot\mathbf{u})$ and by using the incompressibility constraint $\nabla\cdot\mathbf{u} = 0$, the governing equations subsequently read

$$\frac{\partial \mathbf{u}}{\partial t} + \mathbf{u}\cdot\nabla\mathbf{u} + \nabla\tilde{p} + \nu\nabla\times\omega = \mathbf{f} \quad \text{in } \Omega, \tag{13}$$

$$\omega - \nabla\times\mathbf{u} = \mathbf{0} \quad \text{in } \Omega, \tag{14}$$

$$\nabla\cdot\mathbf{u} = 0 \quad \text{in } \Omega, \tag{15}$$

where, in the particular case of the two-dimensional problem, $\mathbf{u}^T = [u_1, u_2]$ represents the velocity vector and $\mathbf{f}^T = [f_1, f_2]$ the forcing term per unit mass (if applicable) and ν the kinematic viscosity.

The generalized kinematic pressure $\tilde{p}$ is related to the kinematic pressure p by

$$\tilde{p} = p - \nabla\cdot\mathbf{u}\,. \tag{16}$$

On the continuous level, due to (15) both pressures coincide, but at the discrete level $\tilde{p}$ may differ from p.

Time integration

The time-integration method that has been used is the θ-scheme. Applying this integration scheme to the model equation

$$\frac{\partial \mathbf{u}}{\partial t} = \mathbf{F}\,(\mathbf{u}, x, t)\,, \tag{17}$$

results into:

$$\frac{\mathbf{u}-\mathbf{u}_0}{\Delta t} = \theta\mathbf{F} + (1-\theta)\mathbf{F}_0. \tag{18}$$

In the latter equation, the subscript "0" indicates that the value of the corresponding variable is known from the previous time step. Consequently, the variable Δt is nothing else than $\Delta t = t - t_0$. All computation are initiated by solving the Stokes problem at the first iteration step.

By varying the parameter θ, different temporal accuracies can be obtained. By taking $\theta = 1$, the time integration reduces to backward Euler which is first order $O(\Delta t)$ accurate in time. Setting $\theta = 0$ generates the explicit, first order forward Euler method, which due to the orthogonality of the basis functions leads to a diagonal matrix. The second order $O(\Delta t^2)$ time integration scheme of Crank-Nicolson can be obtained by selecting $\theta = 1/2$. Since the Crank-Nicolson scheme ($\theta = 1/2$) has no damping, small round-off errors persist in the final solution. Therefore, one often takes $\theta = 1/2 + O(\Delta t)$. With this choice, the temporal accuracy remains second order. Moreover, numerical evidence revealed that adding the small factor of order Δt effectively damps the small waves in spectral element simulations.

Since the θ-scheme is unconditinally stable with the choice $1/2 \leq \theta \leq 1$, one often uses the backward Euler scheme ($\theta = 1$) in combination with a large time step to obtain steady state solutions. In order to obtain time-accurate solutions, the backward Euler scheme is not appropriate since it would require prohivitive small times steps and introduces first order artificial diffusion in the discrete system. Therefore, one resorts to second order (or higher) formulations. As stated above, a preferred choice for the parameter θ then becomes $\theta = 1/2 + O(\Delta t)$.

Linearization of the non-linear terms

Before the least-squares principles can be applied and the corresponding weak form discretized with spectral elements, the convective term $\mathbf{u} \cdot \nabla \mathbf{u}$ must be linearized. To this end, one can use a Picard (e.g. successive substitution)

$$\mathbf{u} \cdot \nabla \mathbf{u} \approx \mathbf{u}_0 \cdot \nabla \mathbf{u}, \tag{19}$$

or a Newton linearization

$$\mathbf{u} \cdot \nabla \mathbf{u} \approx \mathbf{u}_0 \cdot \nabla \mathbf{u} + \mathbf{u} \cdot \nabla \mathbf{u}_0 - \mathbf{u}_0 \cdot \nabla \mathbf{u}_0. \tag{20}$$

In the latter two equations, the subscript "0" indicates that the value of the corresponding variable is known from the previous iteration step.

Although Newton linearization converges faster, Picard performs better in the presence of large gradients as will be the case for the lid-driven cavity flow discussed hereafter. So the following linearized momentum equation is obtained:

$$\begin{aligned} &\frac{\mathbf{u} - \mathbf{u}_0}{\Delta t} + \theta \left(\mathbf{u}_0 \cdot \nabla \mathbf{u} + \nabla p + \nu \nabla \times \omega - \mathbf{f} \right) = \\ &\quad (\theta - 1) \left(\mathbf{u}_0 \cdot \nabla \mathbf{u}_0 + \nabla p_0 + \nu \nabla \times \omega_0 - \mathbf{f}_0 \right) \end{aligned} \tag{21}$$

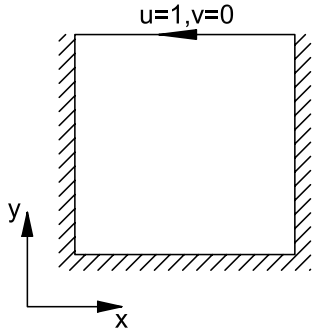

Fig. 1 The problem setup for the lid driven cavity problem.

The least-squares formulation now becomes: Find $\mathbf{u}, p, \omega \in H^1(\Omega)$ which minimizes the functional in the absense of body forces

$$\begin{aligned} &\mathcal{I}(\mathbf{u}, p, \omega) = \|\nabla \cdot \mathbf{u}\|_0^2 + \|\omega - \nabla \times \mathbf{u}\|_0^2 + \\ &\left\| \tfrac{\mathbf{u} - \mathbf{u}_0}{\Delta t} + \theta \left(\mathbf{u}_0 \cdot \nabla \mathbf{u} + \nabla p + \nu \nabla \times \omega \right) - \right. \\ &\left. (\theta - 1) \left(\mathbf{u}_0 \cdot \nabla \mathbf{u}_0 + \nabla p_0 + \nu \nabla \times \omega_0 \right) \right\|_0^2 . \end{aligned} \tag{22}$$

Variational analysis with respect to the four unknowns $\mathbf{u}$, p and ω in (22) leads to the symmatric positive definite system (9). In the present work, system (9) is discretized with conforming spectral elements. To this end, a nodal representation based on the Legendre polynomials has been used to expand the approximate solution[4,8,9] .

4. The lid driven cavity test case

For several years, the lid-driven cavity flow is considered as one of the classical test cases for the assessment of numerical methods and the validation of incompressible Navier-Stokes codes. The lid driven cavity test case deals with a flow in a square box ($[0,1] \times [0,1]$) for which the velocity is zero on three of the sides and is tangent to the fourth side with a constant value equal to 1 (see Figure 1). Because of the discontinuity of the velocity at the two upper corners, the solution of the Navier-Stokes equations becomes singular at these corners. In particular, the vorticity and pressure become infinite. The presence of the sharp gradients of the variables and the singularities at these corners make the lid driven cavity flow a difficult test case. This is particularly true for high-order methods since the sharp gradients might render the computational method unstable whereas low order methods tend to smooth these steep gradients.

In spite of these difficulties and of its physically unrealistic character due to the discontinuous velocity,

the lid driven cavity flow is widely used for evaluating incompressible flow solvers. As a result, a large part of the computations of this test case are motivated by the validation of a novel method rather than to obtain a physical insight in this flow problem. Recently, Botella and Peyret[12] performed a very accurate simulation of the cavity flow in order to produce new benchmark results. To obtain these accurate benchmark results, Botella and Peyret[12] used a Chebyshev collocation method (with varying polynomial order from 128 to 160) to calculate a sufficiently smooth solution by removing the leading part of the singularity from the solution. The latter is determined from an asymptotic expansion of the solution of the Navier-Stokes equations in the vicinity of the corners, by taking the first terms of the expansion into account. Such a technique has already been used in association with Chebyshev methods for the Stokes[25] and Navier-Stokes equations at relatively small values of the Reynolds number.[26] Since the results of Botella and Peyret[12] are the most accurate benchmark results for the lid driven cavity flow, they are also used in the present study.

The simulations are performed at a Reynolds number of 1000, based on the length of the cavity and the speed of the moving lid. This Reynolds number is the standard benchmark test case and it is known that for this Reynolds number a steady solution exists. The velocity boundary conditions are indicated in Figure 1. The arbitrary pressure constant is set to zero at the point $(0.5, 0)$. The geometry has been discretized with a grid consisting of 64 spectral elements. The order of the spectral elements used for the numerical simulations is $N = 4$ and $N = 8$ (see Figure 2). No regularization of the corner singularities has been applied, which makes this tes problem a severe test problem for higher order schemes.

The backward Euler integration scheme has been used. Moreover, it has been assumed that a steady state solution is obtained if the L_2-error of the difference between two successive iterations, which is defined in equation (23), has decreased five orders of magnitude. This error is defined in the following way:

$$L_2\text{-error} = \|\mathbf{u} - \mathbf{u}_0\| \tag{23}$$

where $\mathbf{u}$ and $\mathbf{u}_0$ represent the value of the unknown variable and its value that is known from the previous time level, respectively.

Numerical results

The results of the lid driven cavity problem, obtained at $Re = 1000$ with the Picard linearization, are shown in Figures 3 to 6. As was discussed above, typical for this benchmark problem are the vorticity and pressure singularities near the upper corners of the cavity. To illustrate this, the contour plot of the vorticity and pressure are shown in Figure 3a and 3b, respectively. In these figures, one can clearly observe the large vorticity gradients at the upper corners of the cavity. Similarly, one can also observe, in Figure 3b, the low and high pressure region near the right and left corner of the cavity, respectively. The streamline pattern of the flow can be found in Figure 3c. Typical for the cavity benchmark problem, at this Reynolds number, are the two recirculating regions in the lower corners. All the results, depicted in Figure 3 are obtained with the least-squares spectral element method by using the spectral elements of order $N = 8$.

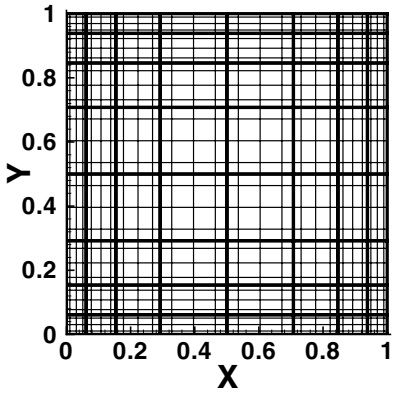

a) The cavity grid of order $N = 4$

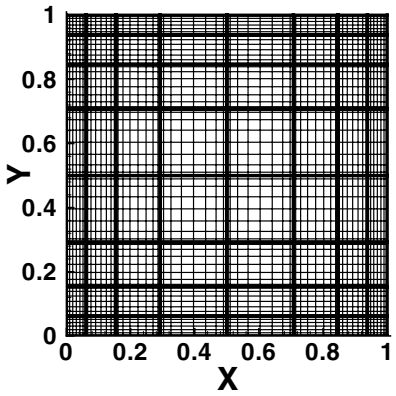

b) The cavity grid of order $N = 8$

Fig. 2 The spectral element grids of order $N = 4$ and $N = 8$ used for the lid driven cavity problem.

In order to further assess the quality of the least-squares formulation, a horizontal ($y = 0.5$) and vertical ($x = 0.5$) cut has been made and the velocity components, vorticity and pressure values are compared with the benchmark results of Botella and Peyret.[12] The results, obtained at the different cross-sections, are shown in Figures 4 to 6. In these figures, the solid and dotted line represent the least-squares spectral element solution obtained at a polynomial degree of $N = 8$ and $N = 4$, respectively. The square symbols denote the benchmark results.

The results of the vertical cut are shown in Figure 4.

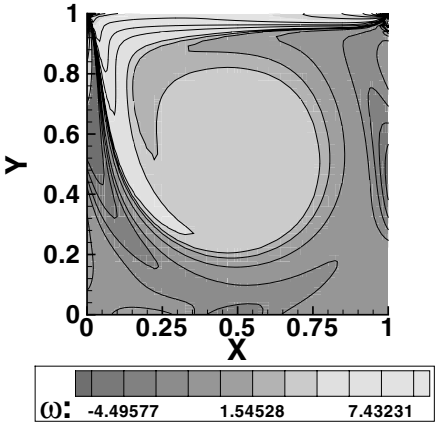

a) The iso-vorticity pattern

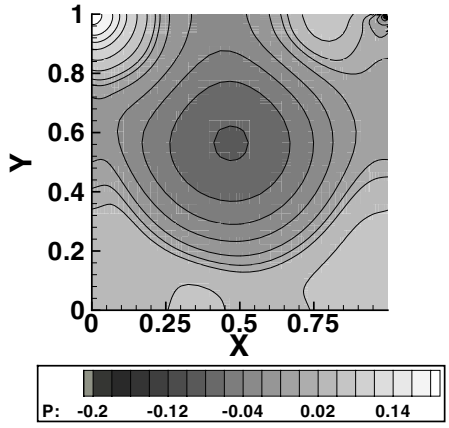

b) The iso-pressure pattern

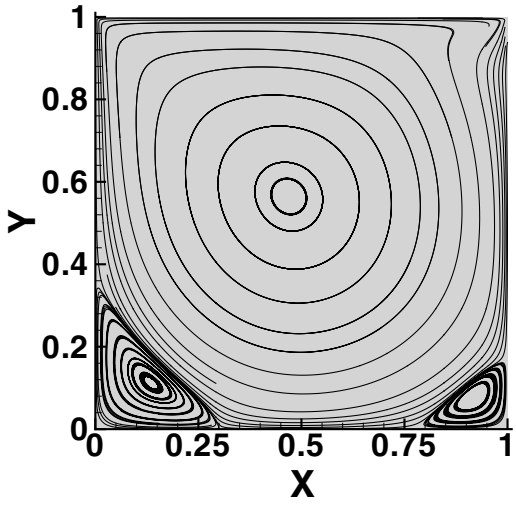

c) The streamline pattern

Fig. 3 The streamline, iso-vorticity and iso-pressure patterns inside the cavity. The results are obtained by using the least-squares spectral element method of order $N = 8$ at $Re = 1000$.

The results are extracted from the two computations along the vertical line located at $x = 0.5$. Figure 4a depicts the velocity component in $x-$direction along this vertical cut. Visual inspection reveals that the numerical solution obtained with the polynomial degree $N = 8$ is much better than the results obtained with the polynomial degree $N = 4$. The result obtained with the lowest polynomial degree only reveals the trend of the simulation but it is clear that the grid and polynomial degree are too coarse to capture the full details of the lid driven cavity problem.

Visual inspection suggests that the results obtained with the spectral elements of order $N = 8$ are located on top of the benchmark results. Analyzing these results in more detail reveals that the simulation with the highest polynomial degree $N = 8$ has a relative error with respect to the benchmark results of approximately 5%. Note that the least-squares simulation was done on a computational grid consisting of approximately $(8 * 9)^2$ GLL collocation points, whereas the benchmark results are obtained on a computational grid consisting of approximately $(160)^2$ Chebyshev-Gauss-Lobatto collocation points. Hence, with only a fifth of the number of collocation points, it is possible to approximate the solution with an absolute error of the order of 10^{-3}. As suggested in Figure 4a, the absolute and relative errors will be higher for the simulation with the polynomial degree of $N = 4$. Moreover, the relative and absolute error are approximately 25% (with a maximum of 55%) and the order of 10^{-2} to 10^{-3}, respectively. Similar observations can be drawn regarding the vorticity (Figure 4b). Moreover, investigating the relative and absolute errors reveals that the most accurate simulation, obtained with the eighth order spectral elements, results in a relative error for the vorticity of approximately 5% and an absolute error of the order of 10^{-2} to 10^{-3}. The results obtained at the polynomial order of $N = 4$ are not sufficiently accurate since a relative error of approximately 15% (with

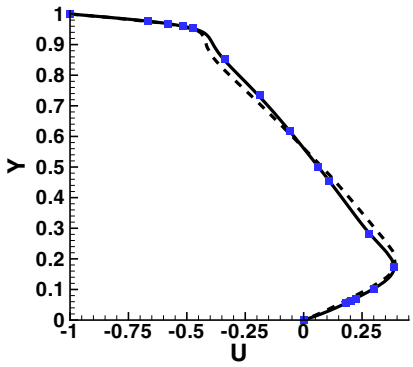

a) The velocity component in $x-$direction at $x = 0.5$

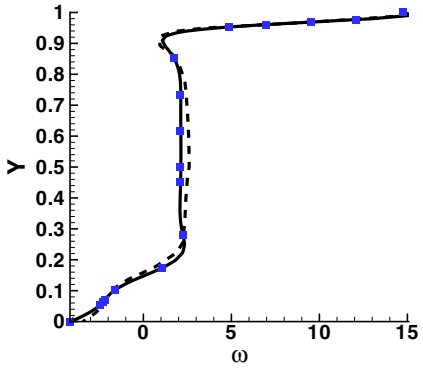

b) The vorticity at $x = 0.5$

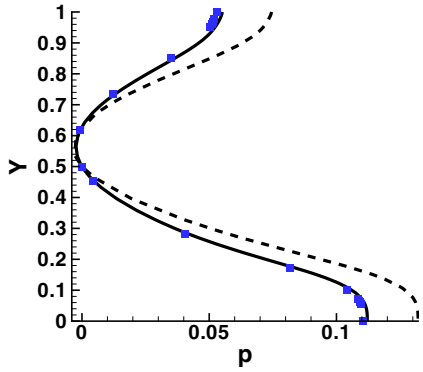

c) The pressure at $x = 0.5$

Fig. 4 The comparison between the benchmark results (at $x = 0.5$) of Botella and Peyret[12] and the results obtained with the least-squares spectral element method at $Re = 1000$.

a maximum of 55%) has been found. An absolute error of the order of 10^{-1} has been found for the latter simulation. The results for the pressure are shown in Figure 4c. The large difference between the simulation obtained at polynomial degree $N = 4$ and $N = 8$ can be clearly observed in this figure. The simulation obtained at a polynomial degree $N = 4$ largely overpredicts the value of the pressure near the solid walls (e.g. at $y = 0$ and $y = 1$). Consequently, a relative error ranging from $\pm 25\%$ to $\pm 55\%$ has been found. Since the pressure constant was not known a priori, the pressure-level of both least-squares spectral element formulations has been adjusted afterwards such that the pressure equals zero at the center of the cavity. This is the point $x = 0.5$ and $y = 0.5$. For this reason, the pressure of both simulations equals the benchmark pressure at the location $y = 0.5$. The numerical simulation at $N = 8$ yields better results since a relative error of $\pm 7\%$ has been found. The absolute error was of the order of 10^{-3} to 10^{-4}.

The results for the horizontal cross-section are shown in Figure 5. The results are extracted from the two computations ($N = 4$ and $N = 8$) along the horizontal line located at $y = 0.5$. In Figures 5a and 5b, the velocity component in $y-$direction and the vorticity are shown along this horizontal cut, respectively. In these figures one can observe that the results of the simulation obtained at $N = 8$ are better than the results obtained at $N = 4$. Moreover, the comparison with the benchmark results indicates that a better agreement is found for the data inferred from the horizontal cut than from the vertical cut since the relative error for the velocity and vorticity, obtained at $N = 8$, is now approximately 3% and 1%. The relative errors for the velocity and vorticity, obtained at the polynomial degree $N = 4$, are approximately 15% (with maximum of 45%) and 5% (with maximum of 9%), respectively. These large relative errors confirm the idea that the polynomial degree $N = 4$ is not sufficient on the present spectral element grid to obtain accurate results. The results obtained at $N = 4$ only give an indication of the behavior but miss some of the essential details. Similar to the pressure, extracted from the vertical cut (Figure 4c), one can also observe that the pressure extracted from the horizontal cut (Figure 5c) shows a large difference between the two numerical simulations. The simulation at $N = 8$ performs much better than the simulation obtained at $N = 4$. The numerical results obtained at the polynomial degree of $N = 8$ show a good agreement in the region near the middle of the cavity and a slight overprediction of the pressure near the solid walls. Indeed a relative and absolute error of approximately 4% and of the order of 10^{-3} has been found for the $N = 8$ simulation, whereas the $N = 4$ simulation displays a relative error of approximately 35% and an absolute

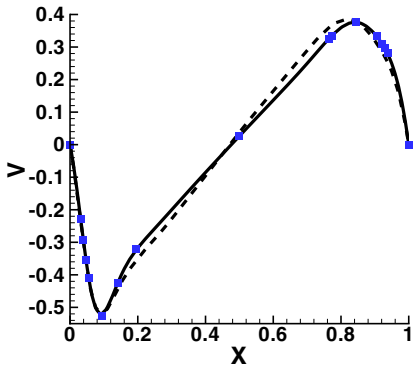

a) The velocity component in $y-$direction at $y = 0.5$

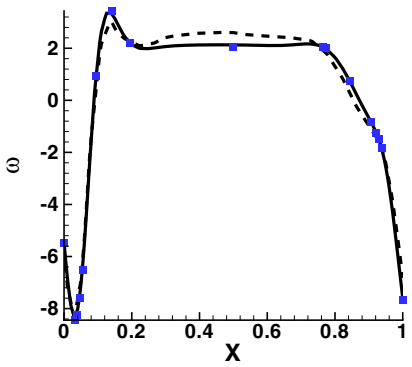

b) The vorticity at $y = 0.5$

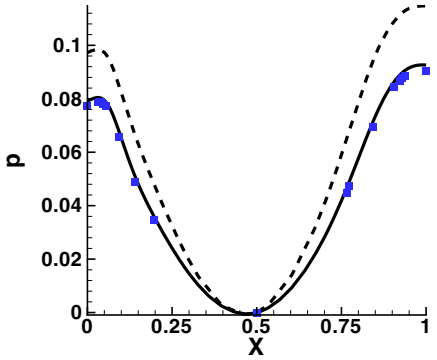

c) The pressure at $y = 0.5$

Fig. 5 The comparison of the vorticity between the benchmark results (at $y = 0.5$) of Botella and Peyret[12] and the results obtained with the least-squares spectral element method at $Re = 1000$.

error of the order of 10^{-2}. It is clear from Figure 5c that the simulation, performed with the fourth order spectral elements, overpredicts the pressure along the whole vertical cut.

The practical applicability of the least-squares method has been further assessed by investigating the vorticity along the moving lid (e.g. at $y = 1$) and at

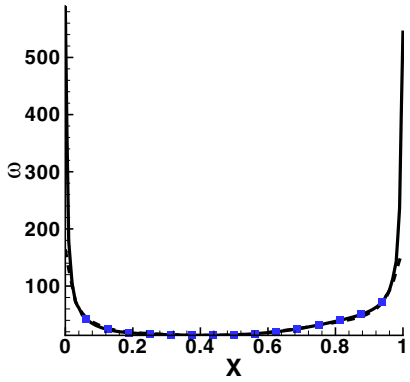

a) The vorticity at the moving lid

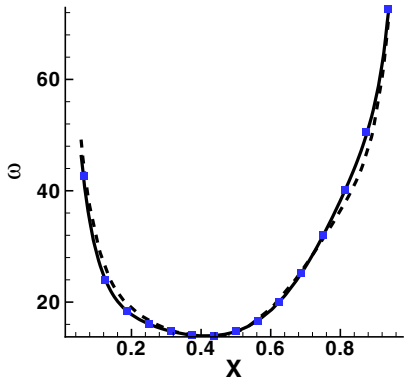

b) A close-up of the vorticity at the moving lid

Fig. 6 The comparison between the results (at $y = 1$) of Botella and Peyret[12] and the results obtained with the least-squares spectral element method at $Re = 1000$.

the secondary vortices. The results along the moving lid are shown in Figure 6. Figure 6a displays the numerical results obtained for the two polynomial degrees. Due to the scale of this figure, one might get the impression that both simulations yield good results. However, scrutinizing these results (see Figure 6b) reveals that only the numerical results obtained with the high polynomial approximation order $N = 8$ show a good agreement since the relative error is below 2% and the absolute error is of the order of 10^{-1} to 10^{-3}.

The results for the secondary vortices are listed in Table 1. The location of the lower left and lower right secondary vortex can be found in the second and third column of this table. The columns four and five list the vorticity at the corresponding location obtained with the polynomial degree of $N = 4$ and $N = 8$, respectively. In the last column, the benchmark results of[12] can be found. These latter results are obtained with a polynomial degree of $N = 160$. In Table 1, one immediately observes the large difference between the benchmark results (column six)

Vortex Location	x	y	ω $(N=4)$	ω $(N=8)$	ω_{ref} $(N=160)$
Lower left	0.1360	0.1118	-0.973271	-1.102420	-1.109789
Lower right	0.9167	0.0781	-0.275997	-0.350858	-0.3522861

Table 1 The intensities of the lower left and right secondary vortices at $Re = 1000$. The results are obtained with the least-squares spectral element method (with the polynomial degree of $N = 4$ and $N = 8$) and compared with the benchmark results of[12]

and results obtained with the least-squares spectral element method at $N = 4$ (column four). At this polynomial degree, the relative error of the vorticity in the lower left and right vortex is approximately 12% and 21%, respectively. These large relative errors confirm that the polynomial degree $N = 4$ is not sufficient on the present spectral element grid to obtain accurate results. The numerical results obtained at the polynomial degree of $N = 8$ show an excellent agreement. Indeed, the relative error of the vorticity in the lower left and right secondary vortex is 0.7% and 0.4%, respectively. The absolute error is of the order of 10^{-3}.

5. Conclusions

In the present paper, a least-squares spectral element method for the unsteady Navier-Stokes equations has been discussed. Least-squares spectral element methods are based on two important and successful numerical methods being spectral/hp element methods and least-squares finite element methods. In this respect, least-squares spectral element methods seem the best of all worlds since they combine the generality of finite element methods with the accuracy of the spectral methods and also the theoretical and computational advantages in the algorithmic design and implementation of the least-squares methods. Most notably, least-squares methods lead to symmetric and positive definite algebraic systems which circumvent the Ladyzhenskaya-Brezzi-Babuška stability condition and subsequently allow the use equal order interpolation polynomials for all the variables.

The present paper continues the development of the least-squares spectral element methods by concentrating on the application of this method to incompressible flow problems. Consequently, the derivation of the least-squares spectral element fomulation of the velocity-vorticity-pressure form of the unsteady Navier-Stokes equations has been discussed in detail in the present paper. Furthermore, the discretization of the non-linear terms and the time-derivative have also been elaborated upon.

Numerical simulations of the lid driven cavity problem have been performed to asses the quality of the new method. The comparison between the benchmark results (obtained at a Reynolds number of 1000) and the numerical simulation, obtained with the eight order spectral elements, revealed a very good agreement (the relative error and absolute error were of the order of $\pm 5\%$ and 10^{-2} to 10^{-3}, respectively). However, these results were obtained with only one fifth of the number of collocation points that were used for the benchmark simulations and no regularization techniques were employed to achieve the results. This confirms that the least-squares spectral element method, despite its high order, produces globally and locally high order accurate results, even in the presence of singularities. Using a finer spectral element grid and/or increasing the order of the spectral elements will further improve the numerical solution. The main advantage of the least-squares spectral element method compared to its Galerkin counterpart is that the algebraic systems remain symmetric positive definite. This holds even for the least-squares spectral element discretization of the Navier-Stokes equations.

References

[1]Henderson, R., "Adaptive spectral element methods for turbulence and transition," *High-order methods for Computational Physics*, No. 9 in LNCSE, Springer-Verlag, 1999, pp. 225–324.

[2]Karniadakis, G. E. and Sherwin, S. J., *Spectral/hp Element Methods for CFD*, Oxford University Press, 1999.

[3]Couzy, W., *Spectral element discretization of the unsteady Navier-Stokes equations and its iterative solution on parallel computers*, Ph.D. thesis, École Polytechnique Fédérale de Lausanne, 1995.

[4]Proot, M. M. J., *The least-squares spectral element method*, Ph.D. thesis, Delft University of Technology, 2003.

[5]Bernardi, C. and Maday, Y., *Approximations spectrale de problèmes aux limites élliptiques*, Springer-Verlag, 1992.

[6]Maday, Y. and Patera, A. T., "Spectral element methods for the incompressible Navier-Stokes equations," *State-of-the-Art surveys in Computational Mechanics*, edited by A. K. Noor and J. T. Oden, 1989, pp. 71–143.

[7]Bochev, P. B. and Gunzburger, M. D., "Finite element methods of least-squares type," *SIAM Rev.*, Vol. 40, No. 4, 1998, pp. 789–837.

[8]Proot, M. M. J. and Gerritsma, M. I., "A least-squares spectral element formulation for the Stokes problem," *J. Sci. Comput.*, Vol. 17, No. 1-3, 2002, pp. 311–322.

[9]Proot, M. M. J. and Gerritsma, M. I., "Least-squares spectral elements applied to the Stokes problem," *J. Comput. Phys.*, Vol. 181, No. 2, 2002, pp. 454–477.

[10]Proot, M. M. J. and Gerritsma, M. I., "Application of the Least-Squares Spectral Element Method using Chebyshev Polynomials to solve the Navier-Stokes equations," *submitted to Numerical Algorithms*, 2003.

[11]Aziz, A. K., Kellogg, R. B., and Stephens, A. B., "Least-squares methods for elliptic systems," *Math. Comput.*, Vol. 44, No. 169, 1985, pp. 53–70.

[12]Botella, O. and Peyret, R., "Benchmark spectral results on the lid-driven cavity flow," *Comput. Fluids*, Vol. 27, No. 4, 1998, pp. 421–433.

[13]Jiang, B.-N., *The Least-Squares Finite Element Method, Theory and Applications in Computational Fluid Dynamics and Electromagnetics*, Springer-Verlag, 1998.

[14]Bochev, P. B., "Analysis of least-squares finite element methods for the Navier-Stokes equations," *SIAM J. Numer. Anal.*, Vol. 34, No. 5, 1997, pp. 1817–1844.

[15]Bochev, P. B. and Gunzburger, M. D., "A least squares finite element methods for the Navier-Stokes equations," *App. Math. Lett.*, Vol. 6, No. 2, 1993, pp. 27–30.

[16]Bochev, P. B. and Gunzburger, M. D., "Analysis of least squares finite element methods for the Stokes equations," *Math. Comput.*, Vol. 63, No. 208, 1994, pp. 479–506.

[17]Chang, C. L., "An error estimate of the least-squares finite element method for the Stokes problem in three dimensions," *Math. Comput.*, Vol. 63, No. 207, 1994, pp. 41–50.

[18]Chang, C. L. and Jiang, B.-N., "An error analysis of least-squares finite element method of velocity-pressure-vorticity formulation for Stokes problem," *Comput. Methods Appl. Mech. Engrg.*, Vol. 84, No. 3, 1990, pp. 247–255.

[19]Jiang, B.-N., "A Least-Squares finite element method for incompressible Navier-Stokes problems," *Int. J. Numer. Methods Fluids*, Vol. 14, No. 7, 1992, pp. 843–859.

[20]Jiang, B.-N., Lin, T. L., and Povinelli, L. A., "Large-scale computation of incompressible viscous flow by least-Squares finite element method," *Comput. Methods Appl. Mech. Engrg.*, Vol. 114, No. 3-4, 1994, pp. 213–231.

[21]Jiang, B.-N. and Chang, C. L., "Least-Squares finite elements for the Stokes problem," *Comput. Methods Appl. Mech. Engrg*, Vol. 78, No. 3, 1990, pp. 297–311.

[22]Jiang, B.-N. and Povinelli, L., "Least-squares finite element method for fluid dynamics," *Comput. Methods Appl. Mech. Engrg.*, Vol. 81, No. 1, 1990, pp. 13–37.

[23]Jiang, B.-N., "On the least-squares method," *Comput. Methods Appl. Mech. Engrg*, Vol. 152, No. 1-2, 1998, pp. 239–257.

[24]Deang, J. M. and Gunzburger, M. D., "Issues related to least-squares finite element methods for the Stokes equations," *SIAM J. Sci. Comput.*, Vol. 20, No. 3, 1998, pp. 878–906.

[25]Schumack, M. R., Schultz, W. W., and Boyd, J. P., "Spectral method solution of the Stokes equations on nonstaggered grid," *J. Comput. Phys.*, Vol. 94, No. 1, 1991, pp. 30–58.

[26]Schultz, W. W., Lee, N. Y., and Boyd, J. P., "Chebyshev pseudospectral method of viscous flows with corner singularities," *J. Sci. Comput.*, Vol. 4, 1989, pp. 1–24.